doi: 10.1038/nature07234

The increasing intensity of the strongest tropical cyclones

James B. Elsner

Department of Geography, Florida State University

Tallahassee, Florida

Corresponding author address:

Dept. of Geography, The Florida State University

Tallahassee, FL 32306

Tel: 850-877-4039, Fax: 850-644-5913

E-mail: jelsner@fsu.edu

James P. Kossin

Cooperative Institute for Meteorological Satellite Studies

University of Wisconsin-Madison

Thomas H. Jagger

Department of Geography, Florida State University

June 26, 2008

Methods

Figure 1 is a schematic of the procedures used to obtain our main finding of upward trends in the intensity of the strongest tropical cyclones. The analyses and modeling techniques performed in this study are labeled with red text. We use a statistical model to estimate the lifetime maximum wind speed (intensity) for each tropical cyclone over the globe. The model is built using a log-linear regression of the aircraft measured maximum per cyclone wind speed onto the principal components (PC) of brightness temperature profiles measured from infrared satellite sensors looking at 171 cyclones occurring across the North Atlantic in the period 1988–2006. Additional covariates include cyclone latitude (absolute value) and age (number of 3-hr periods for which maximum wind speed exceeded 17 ms^{-1}). The maximum wind represents the highest wind speed estimated by aircraft for each cyclone and may be somewhat lower than the cyclone's lifetime maximum wind speed depending on when the aircraft was flying relative to the lifetime maximum (in less than 6% of the cyclones is the aircraft measured wind speed more than 5 ms^{-1} below the cyclone's lifetime maximum).

The PCs are the time-dependent expansion coefficients of an empirical orthogonal function (EOF) analysis performed on the brightness temperature profiles. Higher, colder cloud-tops are associated with colder brightness temperature. Details and discussions concerning the homogeneity of the satellite data are available in refs. 20–22. Details of the principal component analysis are found in ref. 16. The most significant predictors are the first PC and the age of the cyclone. The first PC tracks the departure from the average profile. Colder than normal cloud-top temperatures associated with stronger tropical cyclones are associated with negative values of the first PC. The data set used to build the model is similar to that used in ref. 16. The final regression model includes PCs 1, 3, 4, and 5 as well as cyclone latitude and age.

Model diagnostic plots are shown in Fig. 2. The model explains 69% of the variation in the logarithm of observed lifetime maximum wind speed and the distribution of the observed and model estimates have similar positively skewed distributions as expected

with wind speeds bounded below by zero. There is no autocorrelation in the model residuals. The model is modified from ref. 16 to better account for the skewness in the observed wind speeds. In fact, the model residuals plotted against the predicted maximum wind speed (Fig. 3) show relatively constant variance across the range of predicted values lending support to the log-linear model. There is no trend in the regression model residuals over time (Fig. 4) indicating that changes in tropical cyclone reporting protocols, such as changes in the method for reducing aircraft flight-level winds to the surface (ref. 23), do not affect the results. Moreover there is no dependence of model residuals on satellite view angle (Fig. 5).

The statistical model is subsequently used to estimate lifetime maximum wind speeds for 2097 cyclones around the globe during the period 1981–2006. These satellite-derived wind speeds are estimated at the time of the best-track lifetime maximum wind speed. By construction (regression model), the satellite-derived maximum wind speeds will be less dispersed (lower variance) than observed wind speeds so the trend results presented in this study based on quantile regression are conservative. The time period is chosen so as to have relatively constant seasonal-averaged satellite view angle (Fig. 6).

With the advent of the Meteosat-7 satellite there was improvement in view angle (smaller) for cyclones over the Indian Ocean. A satellite positioned at a large angle relative to the zenith of the tropical cyclone (view angle) will report colder cloud-top temperatures (ref. 24) and thus the statistical model will produce an erroneously high wind speed. Figure 7 shows the seasonal averaged view angle over the southern Indian Ocean by year and the corresponding values of the first PC. There is an abrupt upward shift in the values of the PC corresponding to the improvement in view angle. We therefore adjust all the pre-1998 PCs by adding the difference in means between the two periods (1981–97 and 1998–2006) (see the red line). This also has the effect of shifting the trends estimated from the quantile regression to be more in line with the trends estimated from the quantile regression using the best-track data (Fig. 8). Starting with the year 1981 avoids the largest satellite view angles for the South Pacific Ocean tropical cyclones. Including the three cyclones of 1981, when the view angle was still relatively large, has

no influence on the results.

In the exploratory analysis we use box plots representing the distribution of lifetime maximum wind speeds for each year and, for illustration, draw trend lines through the median, upper quartile values, and extreme values. The median value is depicted with a horizontal dash near the middle of the box, the upper quartile value is depicted as the top of the box, and the extreme value is depicted as the horizontal dash at the end of the "whisker" (dashed vertical line extending from the top of the box). The extreme values are based on 1.5 times the interquartile range from the median, which represents about 95% of the data values. If there are no wind speeds beyond this range then the annual maximum is used instead. This occurs in 3 of the 26 years. The trend line through these extremes is upward. We make no attempt to ascertain the significance of this trend in this analysis. Instead we use quantile regression.

Quantile regression is an extension of median regression based on estimating the value of the parameter vector $\boldsymbol{\beta}$ from the set of allowable vectors that minimizes the mean loss function

$$L_\tau(\boldsymbol{\beta}, \boldsymbol{y}) \quad = \quad \frac{1}{n}\sum_{i=1}^{n} p_\tau\left(y_i - \mu(\boldsymbol{x_i}, \boldsymbol{\beta})\right) \tag{1}$$

where $y_i; i = 1, ..., n$ are the response values, μ is the estimate of the τ quantile, and $\boldsymbol{x_i}$ and $\boldsymbol{\beta}$ are the covariate vector and parameter vector, respectively. The loss function is $p_\tau(\cdot)$, where

$$p_\tau(z) = |z| \left\{\tau \cdot I(z > 0) + (1 - \tau) \cdot I(z < 0)\right\} \tag{2}$$

and $I(x)$ is the indicator function, which is one when x is true and zero otherwise. The loss function is non negative taking a minimum value of zero only when $z = 0$.

Given a series of samples with μ constant (intercept-only model), the resulting value of β that minimizes the total loss function occurs only when μ is equal to the τ quantile of the response. If the model fits well, a plot of the fitted values versus the actual values will show that τ percentage of observed values should be less than the fitted values, with $1 - \tau$ percentage of the observed values greater than the fitted values (ref. 25). The total loss function is an unbiased sample estimate of the expected value of $p_\tau\left(Y - \mu(\boldsymbol{x} \cdot \boldsymbol{\beta})\right)$,

and the minimization over $\boldsymbol{\beta}$ is a consistent estimate of the minimizer of this expected value. For the fit we choose a linear model for the regression function of the form

$$\hat{\mu} = \beta_0 + \beta_1 \cdot \mathrm{Year}_i, \tag{3}$$

where Year_i as the covariate is the calendar year in which the cyclone's maximum wind speed was observed. The relatively short record length (26 years) limits our consideration to a linear trend model. We also replace Year with annual global sea-surface temperature (SST) as a covariate.

All statistics were performed using R (ref. 26) and the quantile regression package (quantreg) (ref. 27).

Figure 1 | Schematic of the procedures used to obtain the main result of our study.

Figure 2 | Model diagnostic plots. The model predicted wind speed distribution versus the observed wind speed distribution for the set of cyclones used to build the log-linear regression model. The autocorrelation function indicates no correlation in the residuals between cyclones. The distribution of the predicted wind speeds is also shown as a box plot.

Figure 3 | Model residuals versus predicted wind speed. Predicted lifetime maximum wind speeds are grouped into deciles and box plots show the variation in the residuals for each decile level. The range of residuals is noted by the box and whisker lengths. There is no systematic variation in the range as function of predicted wind speed.

Figure 4 | Model residuals versus satellite view angle. The view angle in degrees from zenith is relative to the position of the tropical cyclone at its maximum intensity. View angles are grouped into deciles and box plots show the variation in the residuals for each decile level. There is no systematic variation in the range or trend in central tendency of model residuals across the range of view angles.

Figure 5 | Model residuals versus year. There is no systematic variation or trend in model residuals over time.

Figure 6 | Satellite view angle. The view angle in degrees from zenith is relative to the position of the tropical cyclone at its lifetime maximum intensity.

Figure 7 | Principal component 1 and satellite view angle over the southern Indian Ocean. The view angle in degrees from zenith is relative to the position of the tropical cyclone at its maximum intensity. PC 1 is the most important predictor in the log-linear regression model for satellite-derived tropical cyclone wind speeds. A constant is added to the values

of all PCs for cyclones over the Indian Ocean (northern and southern) in years prior to the advent of Meteosat-7 in 1998 to help correct for the bias in brightness temperatures caused by the large view angle.

Figure 8 | Quantile regression results. Trends in lifetime maximum wind speeds for tropical cyclones over the southern Indian Ocean. Trends are estimated using the uncorrected and corrected satellite-derived lifetime maximum wind speeds and using the best-track lifetime maximum wind speeds.

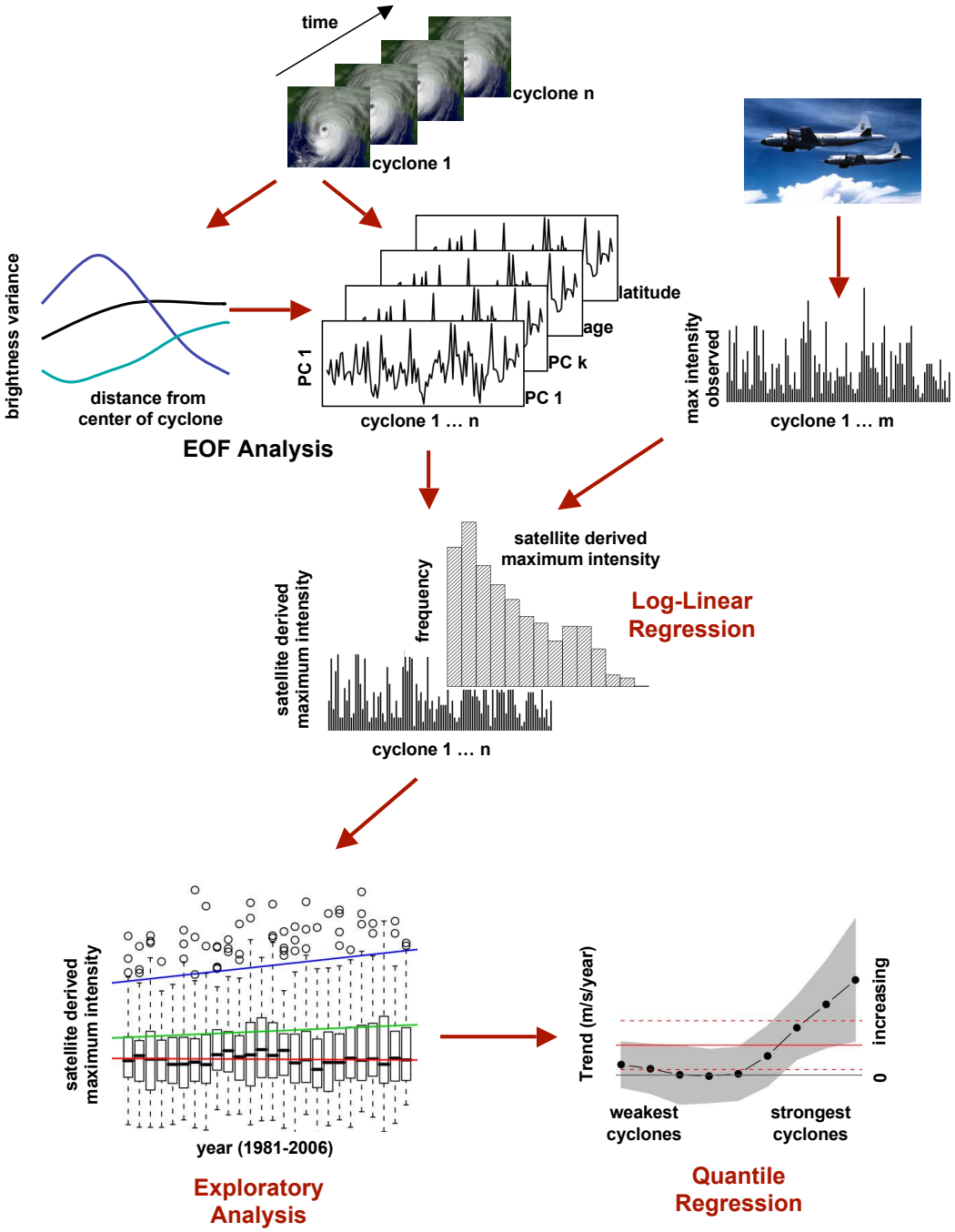
time
cyclone n
cyclone 1
brightness variance
distance from
center of cyclone
latitude
age
PC k
PC 1
PC 1
cyclone 1 … n
EOF Analysis
max intensity
observed
cyclone 1 … m
satellite derived
maximum intensity
frequency
satellite derived
maximum intensity
Log-Linear
Regression
cyclone 1 … n
satellite derived
maximum intensity
year (1981-2006)
Exploratory
Analysis
Trend (m/s/year)
increasing
0
weakest
cyclones
strongest
cyclones
Quantile
Regression

Figure 1:

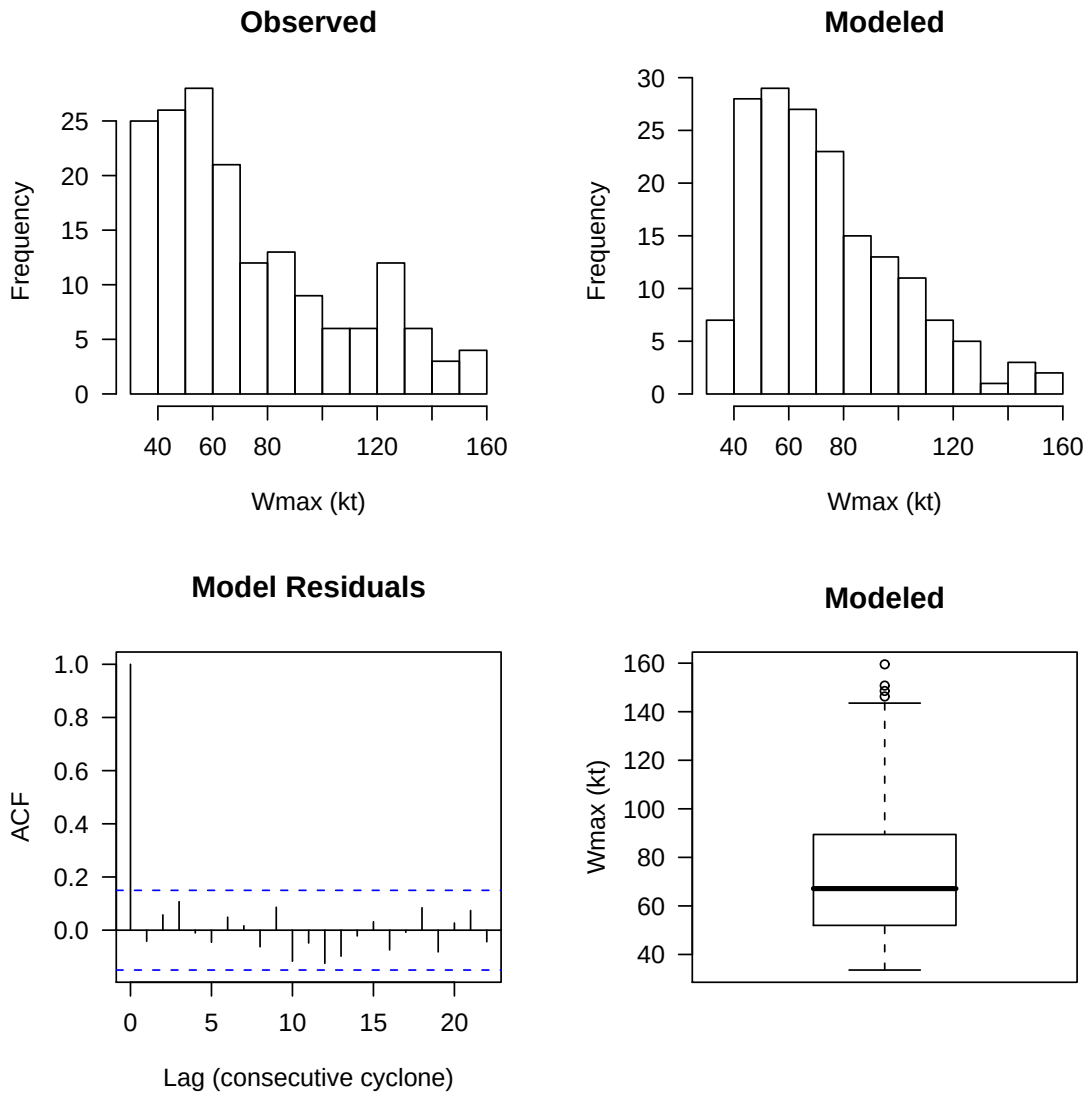
Observed
Frequency
Wmax (kt)
Modeled
Frequency
Wmax (kt)
Model Residuals
ACF
Lag (consecutive cyclone)
Modeled
Wmax (kt)

Figure 2:

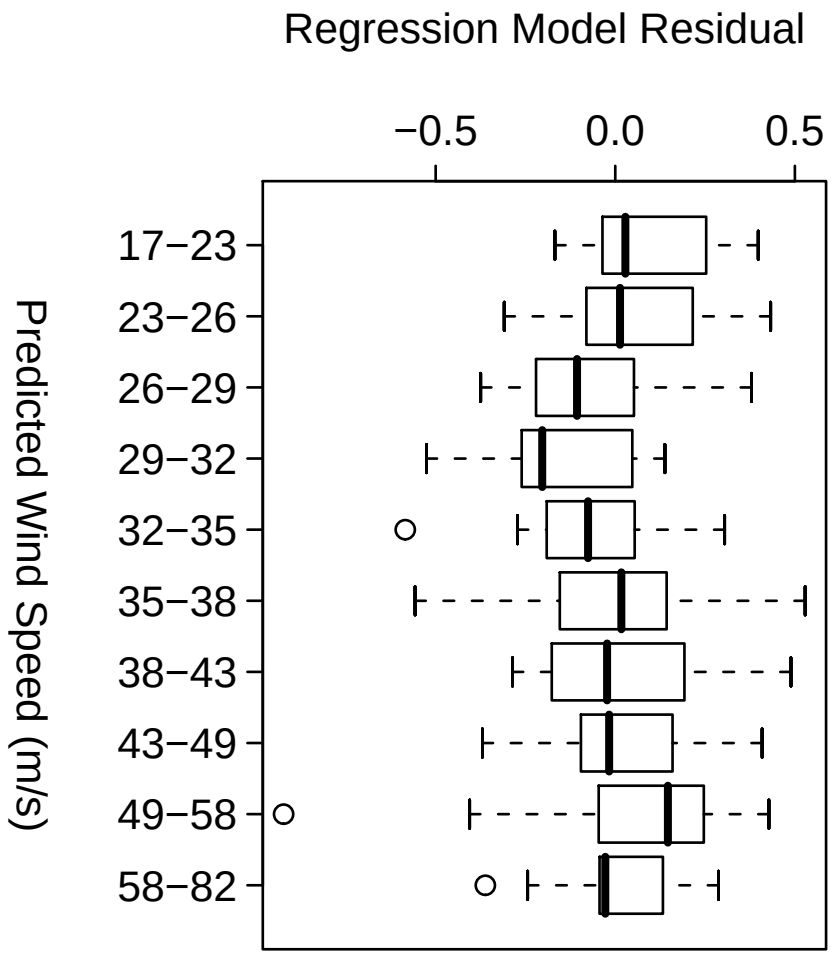
Regression Model Residual
−0.5
0.0
0.5
Predicted Wind Speed (m/s)
17−23
23−26
26−29
29−32
32−35
35−38
38−43
43−49
49−58
58−82

Figure 3:

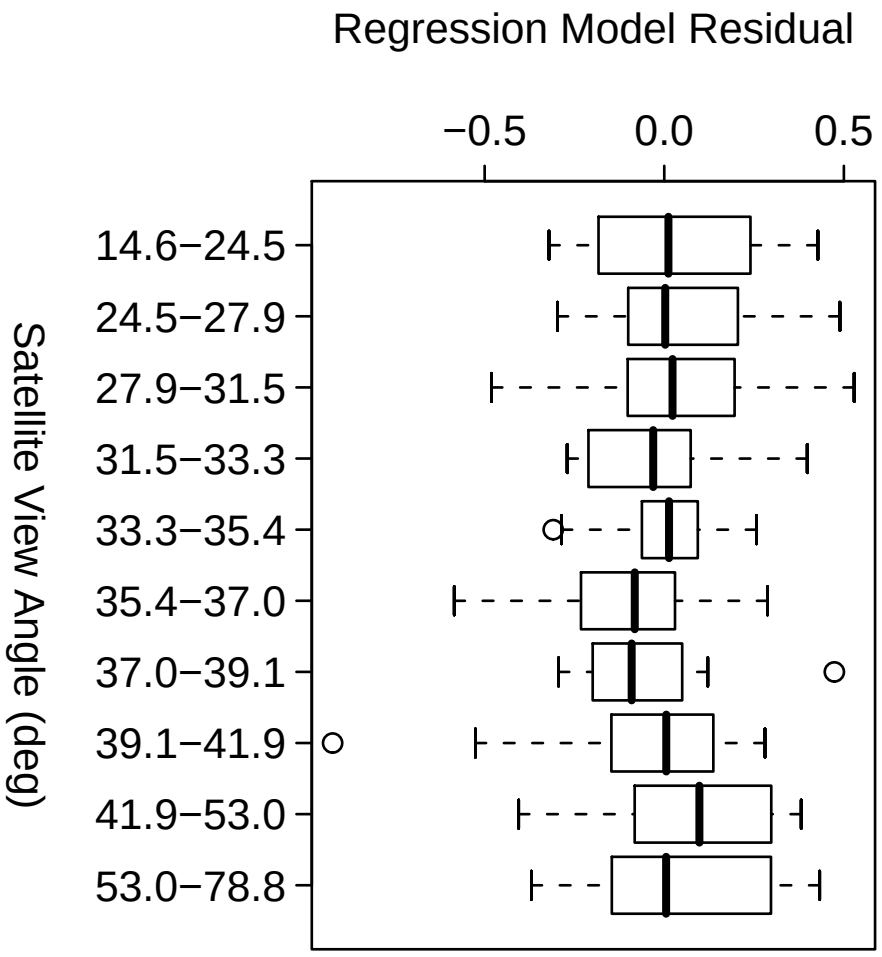
Regression Model Residual
−0.5
0.0
0.5
Satellite View Angle (deg)
14.6−24.5
24.5−27.9
27.9−31.5
31.5−33.3
33.3−35.4
35.4−37.0
37.0−39.1
39.1−41.9
41.9−53.0
53.0−78.8

Figure 4:

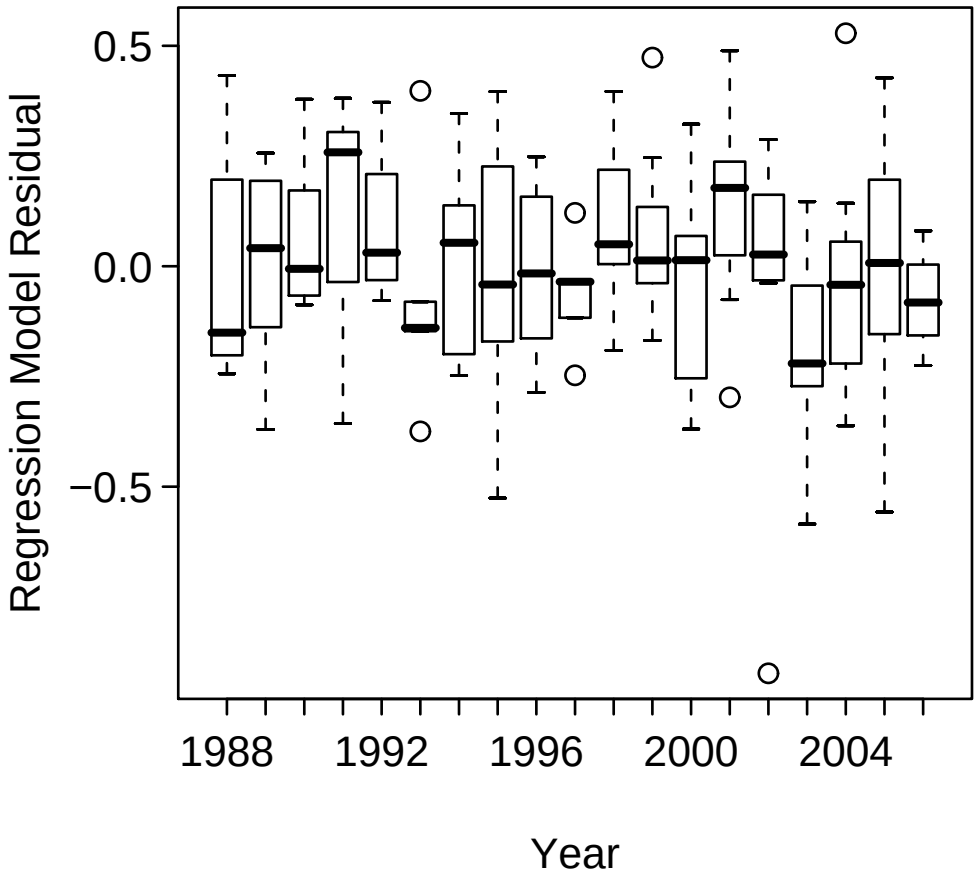
Regression Model Residual
0.5
0.0
−0.5
1988
1992
1996
2000
2004
Year

Figure 5:

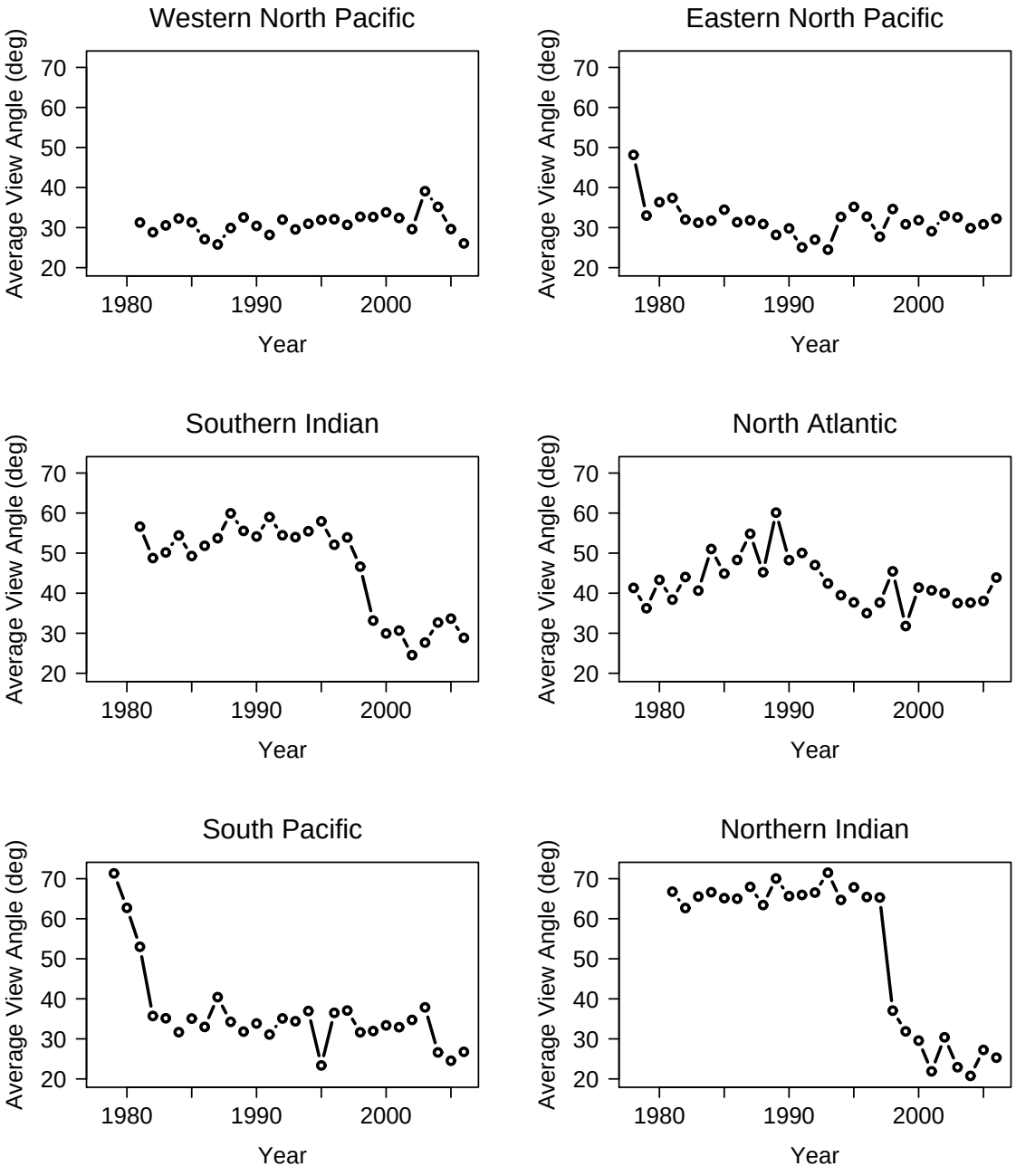
Western North Pacific
Eastern North Pacific
Southern Indian
North Atlantic
South Pacific
Northern Indian
Average View Angle (deg)
Year
20
30
40
50
60
70
1980
1990
2000

Figure 6:

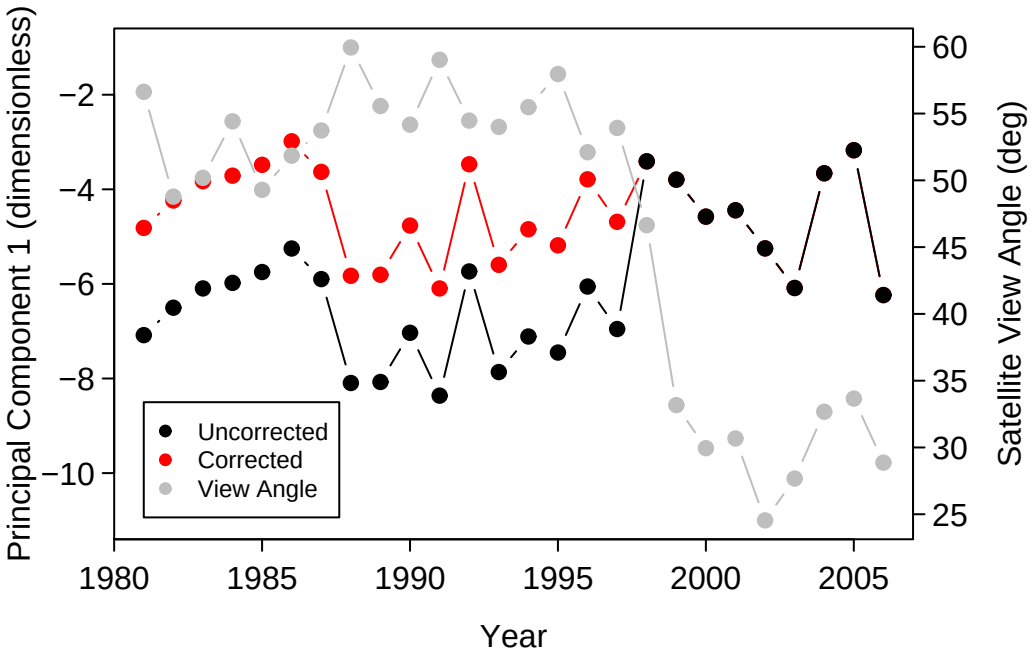
Principal Component 1 (dimensionless)
−2
−4
−6
−8
−10
Satellite View Angle (deg)
60
55
50
45
40
35
30
25
1980
1985
1990
1995
2000
2005
Year
Uncorrected
Corrected
View Angle

Figure 7:

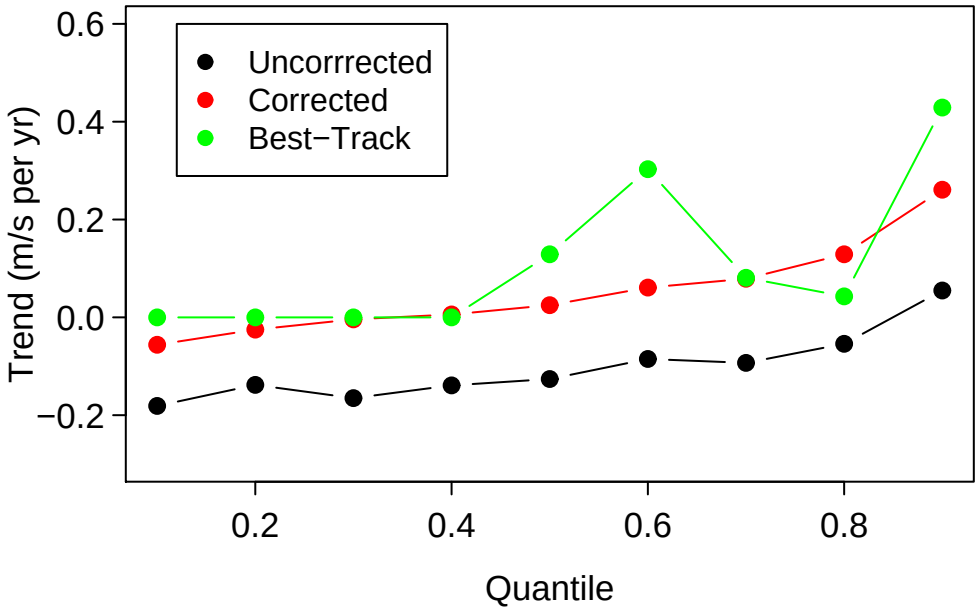
Uncorrrected
Corrected
Best−Track
Trend (m/s per yr)
0.6
0.4
0.2
0.0
−0.2
0.2
0.4
0.6
0.8
Quantile

Figure 8: